Turkish Journal of Electrical Engineering & Computer Sciences

http://journals.tubitak.gov.tr/elektrik/

Research Article

Turk J Elec Eng & Comp Sci
(2013) 21: 1302 – 1317

doi:10.3906/elk-1112-81

Mitigation of SSR and LFO with a TCSC based-conventional damping controller optimized by the PSO algorithm and a fuzzy logic controller

Hasan GHAHRAMANI,* Akbar LAK, Murtaza FARSADI, Hossein HOSSEINI
Department of Electrical Engineering, University of Urmia, Urmia, Iran

Received: 29.12.2011 • **Accepted:** 19.03.2012 • **Published Online:** 12.08.2013 • **Printed:** 06.09.2013

Abstract: The subsynchronous resonance (SSR) phenomenon may occur when a steam turbine-generator is connected to a long transmission line with series compensation. Flexible AC transmission systems (FACTS) devices are widely applied to damp the SSR and low-frequency oscillation (LFO). A thyristor-controlled series capacitor (TCSC) is a commercially available FACTS device that was developed for damping the SSR and LFO. In this paper, 2 control methods for damping the SSR and LFO are added to the TCSC main controller in order to demonstrate that the SSR damping capability of the TCSC can be enhanced by proper modulation of the firing angle. The control methods are presented, namely the conventional damping controller (CDC) and fuzzy logic damping controller (FLDC). The particle swarm optimization (PSO) algorithm is used for searching optimized parameters of the CDC. Fast Fourier transform is carried out in order to evaluate the effect of the TCSC-based FLDC in damping the SSR and LFO. The study system was adopted from the IEEE second benchmark model by altering a part of the fixed series capacitor to the TCSC. The MATLAB/Simulink was used to verify the effectiveness of each control method. The simulation results show that the FLDC has an excellent ability in damping the SSR and LFO in the power system toward the CDC-optimized PSO algorithm.

Key words: Subsynchronous resonance, low-frequency oscillation, thyristor-controlled series capacitor, particle swarm optimization, fuzzy logic controller

1. Introduction

Series capacitive compensation in AC transmission lines provides several advantages; for example, the increased power transfer capability of long transmission lines and improved transient stability of power systems. This is due to the partial compensation of the reactance of the power networks. However, capacitors in series with transmission lines can also lead to subsynchronous resonance (SSR) problems. When this methodology is implemented together with a steam turbine-generator, it can cause the SSR occurrence [1–3]. The flexible AC transmission systems (FACTS) controllers, for instance, the static var compensator, static synchronous series compensator, unified power flow controller, and gate-controlled series capacitor, have been implemented to mitigate the SSR in power networks [4–7]. Among the FACTS devices for transient stability improvement, the thyristor-controlled series capacitor (TCSC) is the most adaptable [8,9]. It can change its obvious reactance smoothly and quickly [10,11]. The TCSC has a great application and ability of exactly adjusting the power flow on a transmission line, alleviating interarea power oscillations [12], damping the SSR, and enhancing the transient stability [13].

*Correspondence: hesen.qehremani@gmail.com

The alleviation effect of the TCSC has the following characteristics [14]:

- The TCSC for the alleviation of power oscillations is more effective than the shunt FACTS devices.
- The TCSC becomes more efficient at controlling power oscillations at higher levels of power exchange.
- The situation of a TCSC on an intertie does not influence the alleviation result.
- The alleviation result is not sensitive to the load features.
- The local modes are not excited when a TCSC is planned to alleviate the interarea modes.

This work shows a detailed analysis of the effect of different TCSC control techniques on the SSR and low-frequency oscillation (LFO) alleviation. The 2 techniques that are used in this paper are explained in the following:

In this paper, output feedback of the conventional damping controller (CDC) optimized by particle swarm optimization (PSO) is designed for TCSC in order to damp the SSR and LFO.

The fuzzy logic damping controller (FLDC) has been one of the popular controllers among the research that has been proposed in power system applications [15,16] such as SSR and LFO alleviation. The benefits of the FLDC over the CDC are that it does not require an exact mathematical model; it can cope with nonlinearity and may be more robust than the optimized CDC [15].

The paper is organized as follows. In Section 2, the subsynchronous resonance phenomenon is explained briefly. The power system structure for the SSR study is clarified in Section 3. In Section 4, the fast Fourier transform (FFT) analysis of the generator rotor speed is demonstrated. The structure of the TCSC is briefly presented in Section 5. In Section 6, the PSO technique is described. The design of the CDC is given and is briefly explained in Section 7. In Section 8, the FLDC design is presented. The simulation results with a detailed comparison between the 2 proposed controllers, the CDC optimized with the PSO algorithm and a fuzzy logic controller (FLC), in 2 cases are included in Section 9. Finally, in Section 10, the results obtained from the previous sections are summarized and conclusions are drawn.

2. Subsynchronous resonance

Due to the destructive effects of the SSR phenomenon, this phenomenon should be introduced and discussed. In this paper, 2 novel auxiliary controllers, the FLDC and adaptive neuro fuzzy inference system controllers, for damping the SSR and LFO are added to the TCSC main controller. Therefore, in this part, the SSR phenomenon will be introduced and analyzed.

Generally, SSR occurs in series-compensated transmission lines [1]. The series compensation of a transmission line can be caused by the excitation of the oscillatory modes of the rotor shaft at a subsynchronous frequency [2]. A series capacitor-compensated power system has a subsynchronous natural frequency (f_e), which is given by:

$$f_e = f_o\sqrt{\frac{X_C}{X_L}} \tag{1}$$

where X_C is the reactance of series capacitor, X_L is the reactance of a compensated line, and f_o is the synchronous frequency of the power system in Hz. At this subsynchronous natural frequency, these oscillatory

modes result in rotor torques and currents at the complementary frequency, f_r as: $f_r = f_o - f_e$. Hence, if f_r is close to one of the torsional frequencies of the rotor shaft, the torsional oscillations will be excited and this condition will result in an unfavorable phenomena, namely the SSR [3]. Generally, the SSR is divided into 2 major parts: self-excitation, which is named by steady-state SSR, and the second is named transient torque or transient SSR. Self-excitation is separated into 2 major parts: the first is the induction generator effect (IGE), and the second is torsional interaction (TI). The IGE is improbable in a series compensated power system. However, the TI and transient SSR mostly occur in series compensated power systems [17,18]. Because the main aim of this paper is to suppress the SSR in a series-compensated transmission line, the proposed controller is designed to solve major SSR problems, transient torque, and TI.

3. Power system study model

To study the effects of the SSR phenomenon and its mitigation, the TCSC should be supplemented with auxiliary controllers that will be added to its main controller. To achieve this goal, a system is needed to investigate the effects of SSR on it. In this part, the system under study, the IEEE second benchmark model (ISBM), is introduced, and briefly explained for the mentioned goal.

For the analysis investigated in this study, the ISBM is used [19]. The system is composed of a synchronous generator supplying power to an infinite bus via 2 parallel transmission lines; it is a single machine infinite bus power network that has 2 transmission lines and 1 of them is compensated by a series capacitor accompanying the TCSC that is shown in Figure 1. In this model, a 600 MVA synchronous generator is attached to an infinite bus, and the rated line voltage is 500 KV, while the rated frequency is 60 Hz. The shaft system consists of 4 masses: the generator (G) and rotating exciter (EX), a high-pressure (HP) turbine, and a low-pressure (LP) turbine. The transmission line is illustrated by a resistance, a reactance, a series fixed capacitive compensation (X_{fc}), and the TCSC with an equivalent reactance ($X_{TCSC}(\alpha)$). The complete mechanical and electrical data for the study system are displayed in [19].

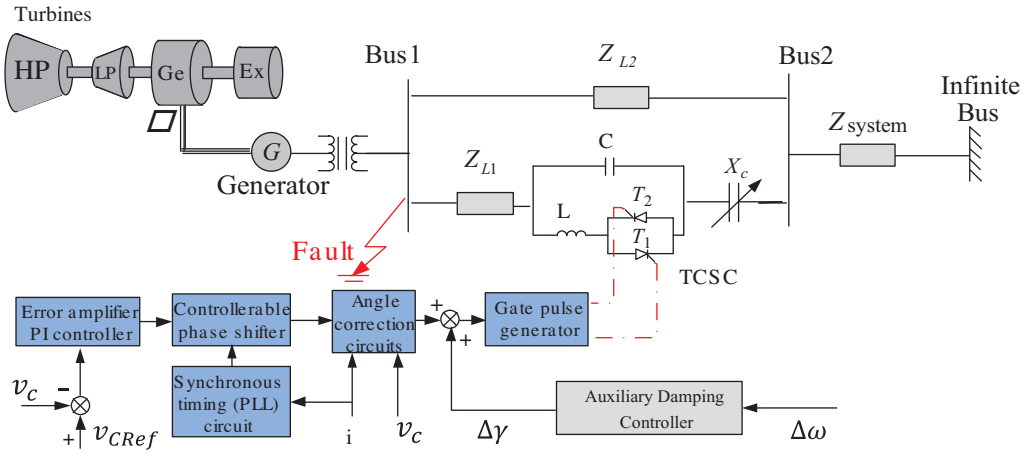

Figure 1. The ISBM combined with a TCSC for SSR analysis.

4. Fast Fourier transform analysis

FFT is one of the most appropriate approaches for achieving the oscillatory modes of the system, which is used in this study to investigate the inherent modes in the ISBM. It should be noted that the TCSC has no inherent

ability for damping the SSR.

For evaluating the dynamic features of the power system, the FFT analysis is achieved using an M-file in the MATLAB program, which is shown in Figure 2. The without damping factor of the SSR modes of the generator rotor shaft, as a function of the percentage of compensation, which means that the ratio of the series capacitive reactance to the line reactance $((X_C/X_L)\times\ 100)$ is shown, is fixed at 55% $((X_{fc}/X_L) = 0.37$ and $(\mathrm{X}_{TCSC}(\alpha)/X_L) = 0.18)$ to excite the oscillatory mode of the generator rotor shaft. The FFT analysis reveals that 3 modes exist in the generator rotor speed, of which 2 of the modes, 25 Hz and 32.5 Hz, are the oscillatory modes of the generator rotor shaft, and the third mode, 1.5 Hz, is the low frequency oscillation. The conqueror mode, which has a subsynchronous frequency, is 25 Hz.

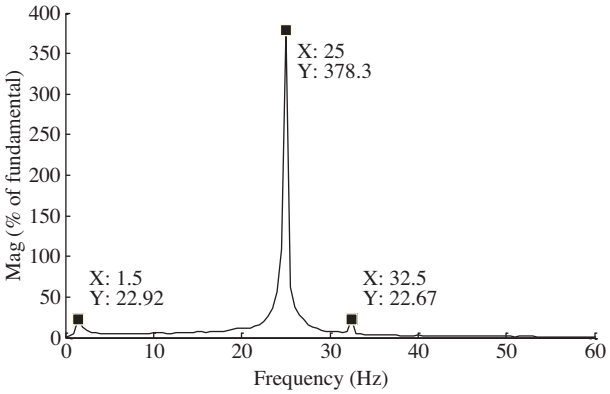

Figure 2. FFT analysis on the generator rotor shaft for verifying the conqueror mode.

To confirm how undesirable this dominant mode is, the FFT analysis of the generator rotor speed is presented at 1–9 s, with a time division of 2 s. The results acquired for the FFT analysis are displayed in Figure 3.

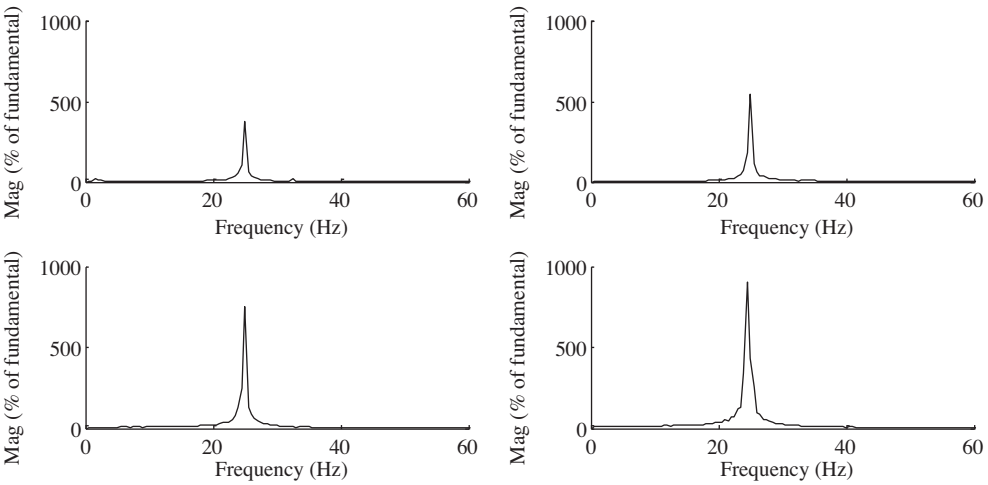

Figure 3. FFT analyses on ω of the generator rotor speed, without a damping controller.

Referring to Figure 3, it can be seen that as the time advances the conqueror mode component increases considerably. Hence, if this continues to intensify, the rotor shaft can seriously damage the mechanical shaft system; thus, there should be a controller in order to alleviation this contrary oscillatory component from the rotor shaft in order to protect the power system.

5. Structure of the TCSC

As mentioned, the TCSC is one of the FACTS devices that are used in this study to mitigate the SSR. Therefore, the structure of the TCSC is introduced in this section. The TCSC is one of the most widely utilized FACTS devices in power systems. It can adjust the impedance smoothly in an extensive range by adjusting the firing angles of the thyristor, and with this ability it can adjust the transmission line impedance to control the power flow, improve the system stability, and enhance the power transfer capacity [8,9].

The basic TCSC is shown in Figure 1. It comprises the series compensating capacitor shunted by a thyristor-controlled reactor (TCR). The basic idea behind the TCSC plan is to provide a continuously alterable capacitor by means of partially cancelling the efficient of the compensating capacitance by the TCR. The TCR at the basic system frequency is a continuously alterable reactive impedance, controllable by a delay angle, and the steady-state impedance of the TCSC is that of a parallel inductor-capacitor (LC) circuit, containing a fixed capacitive impedance, X_C, and an alterable inductive impedance, $X_L(\alpha)$, that is:

$$X_{TCSC}(\alpha) = \frac{X_L(\alpha)X_C}{X_L(\alpha) - X_C} \tag{2}$$

$$X_L(\alpha) = X_L \frac{\pi}{\pi - 2\alpha - \sin\alpha}, X_L \leq X_L(\alpha) \leq \infty \tag{3}$$

$X_L = \omega L$ and α is the delay angle measured from the peak of the capacitor voltage [20,21].

The TCSC thus exhibits a tuneable parallel LC circuit to the line current that is a constant alternating current source. As the impedance of the controlled reactor, $X_L(\alpha)$ is changed to its minimum (ω L) from toward its maximum (infinity). The TCSC decreases its maximum capacitive impedance when a parallel resonance at $X_C = X_L(\alpha)$ is established and $X_{TCSC\ \max}$ theoretically becomes infinite until the minimum capacitive impedance, $X_{TCSC,\min} = X_C = 1/\omega c$.

Decreasing $X_L(\alpha)$ additionally, the impedance of the TCSC, $X_{TCSC}(\alpha)$, becomes inductive, achieving its minimum value of $((X_L(\alpha)X_c)/(X_L(\alpha) - X_c))$ at $\alpha = 0$, where the capacitor is in fact bypassed by the TCR [20,21].

Thus, with the usual TCSC structure, in which the impedance of the capacitor, X_C, is bigger than that of the TCR reactor, X_L, the TCSC has 2 operating ranges around its internal circuit resonance: one is the $\alpha_{Clim} \leq \alpha \leq \pi/2$ range, where $X_{TCSC}(\alpha)$ is capacitive, and the other is the $0 \leq \alpha \leq \alpha_{Llim}$ range, where $X_{TCSC}(\alpha)$ is inductive, as demonstrated in Figure 4. In this paper, the TCSC is used instead of a series capacitor in the ISBM. Hence, the α can be changed around $\pi/2$, and thus there is no internal circuit resonance in the TCSC [20,21].

6. PSO technique

The PSO is a population-based method and is described by its developers as an optimization paradigm that models the social behavior of birds flocking or fish schooling for food. Therefore, PSO works with a population of potential solutions rather than with a single individual [22–24], searching for the optimum solution resumptions unless one of the stopping criteria arrives. The stopping criteria can consist of the below occasions [23]:

1. The definitive maximum iterations are arrived at.
2. There is no further improvement in the optimal solution.

The flowchart of PSO is shown in Figure 5.

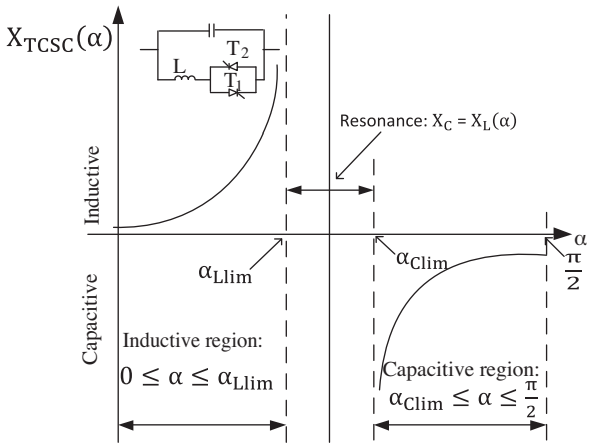

Figure 4. The impedance of the TCSC to the delay angle α variation.

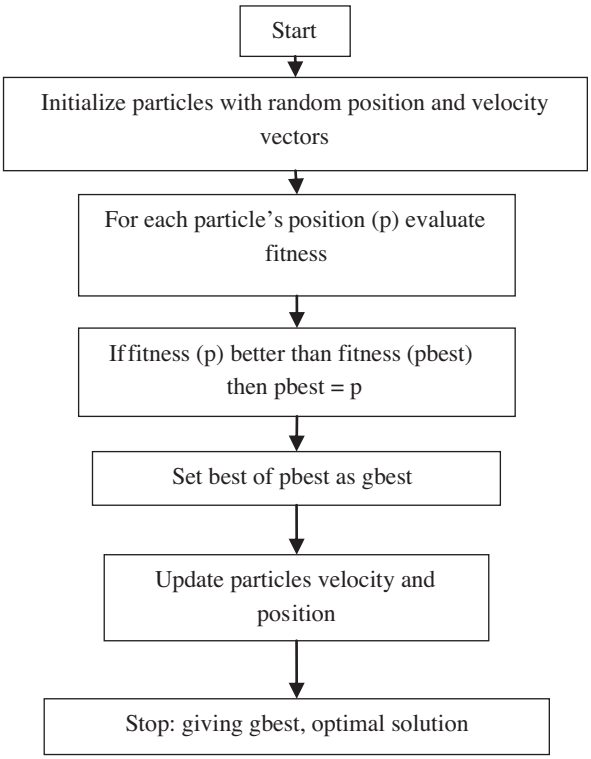

Figure 5. Flowchart of the PSO algorithm procedure.

In the PSO technique, a number of simple entities, the particles, are placed in the search space of some problem or function, and the loop and stability control loop have been used to provide the required control action for the TCSC.

In this paper, the PSO algorithm is selected to tune the K, Tw, T1, and T2 parameters in the CDC. It is clear that because of the importance of damping the SSR and LFO in a short time and also for decreasing the steady state errors in this system, the objective function is presented below:

$$\int_0^{tsim} t\,|\Delta\omega(t)|dt \tag{4}$$

The first step in using PSO (as with each evolution algorithm) is to initialize the CDC parameters (K, Tw, T1, and T2) based on intervals shown in Table 1. The next and main step is to calculate the objective function; a proper function is used in this work (Eq. (4)). The main purpose is to minimize the speed variation $\Delta\omega$. The proposed objective function has a direct relation with $\Delta\omega$; therefore, since minimizing the function makes the speed variation decrease, this means that the process continues to achieve the best possible answer for the CDC parameters.

Table 1 shows the parameters of the CDC that are obtained through the PSO algorithm.

Table 1. The parameters of the CDC that are obtained through the PSO algorithm.

$K = 100$	$0 < K < 150$
$T_w = 20$	$0 < T_w < 40$
$T_1 = 0.1$	$0 < T_1 < 5$
$T_2 = 0.01$	$0 < T_2 < 2.5$

7. Design CDC

The conventional controller is mostly utilized in industry due to its simple control structure [25], ease of design, and low cost. In this study, because the purpose is to alleviate the SSR, the speed deviation of the generator rotor has been employed as the input signal of the conventional controller. As shown in Figure 1, $\Delta\omega$ [pu] has been implemented as an additional signal to alleviate the unstable modes.

The CDC for the SSR consists of 4 blocks [25]: a washout filter, a phase compensator block, limiter block, and a gain block. The washout filter is used to prevent the controller from responding to the steady-state changes of the input signal. The phase compensator block presents the suitable lead–lag features so that producing the damping torque and the corresponding gain of an additional damping controller is specified from methodically utilizing the nonlinear time domain simulation, in order to obtain faster setting time. The limiter block tends to restrict the output of the controller when it is going to decrease or increase from a specific range. As shown in Figure 6, the output of the CDC is therefore sent to the TCSC voltage regulator.

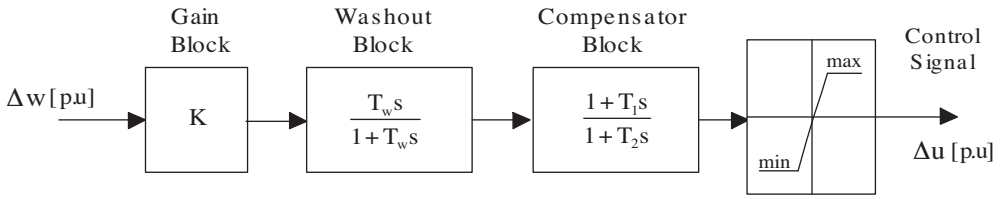

Figure 6. CDC block diagram.

Table 2 shows the necessary information for the PSO algorithm.

Table 2. The parameter settings for the PSO.

Population size	C2	C1	W	Iteration
40	2	2	0.9	15

8. FLDC design for the TCSC

According to the results and explanations provided in Section 4, it is observed that the TCSC does not have an inherent ability for damping the SSR and LFO. Thus, to eliminate this defect, an auxiliary controller must

be added to the TCSC controller system. In the previous section, the CDC optimized with the PSO algorithm is added to the TCSC. In this section, this work is done again using the FLDC. The FLDC has been one of the popular controllers among researchers that has been proposed in the power system application [15,16], such as SSR and LFO alleviation. The benefits of the FLDC over the CDC are that it does not require an exact mathematical model; it can cope with nonlinearity and may be more robust than the optimized CDC [15]. Hence, the first operation of the FLDC has been described, and next, how to apply the FLDC to the control system of the TCSC is explained.

Figure 7 displays a schematic of the supplementary FLDC that is added to the TCSC main control in order to damp the SSR and LFO. In this section, the rotor speed deviation and its derivative ($\Delta\omega$ and ($d\Delta\omega$/dt) = $\Delta\gamma$) are utilized as inputs for the proposed FLDC that is planned based on the Mamadani inference engine.

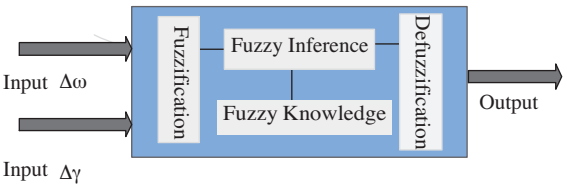

Figure 7. Generalized TCSC supplementary fuzzy controller for subsynchronous resonance damping.

The fundamental construction of the FLDC is classified into 4 sections, namely a fuzzification block, fuzzy knowledge-based block, fuzzy inference engine, and a defuzzification block [26–28].

8.1. Fuzzification

Fuzzification is the process of finding the appropriate membership function to illustrate the crisp data from the power system. The fuzzy inputs include $\Delta\omega$ and $\Delta\gamma$ by investigating the behavior of these input signals under different conditions before and after the fault, and the fuzzy sets for the fuzzy controller are planned. The input signals of the FLDC are scaled using the appropriate component factors. This scaled input information is then transformed into linguistic variables, which can be observed as the labels of the fuzzy sets. Fuzzy sets may be arranged by membership functions. The membership functions can be classified into different forms; for example, linear function, triangular function, trapezoidal function, and exponential function [26–28].

8.2. Fuzzy knowledge-base

The knowledge-base is the main part of a fuzzy controller, which is composed of 2 parts called the fuzzy sets (base data) and fuzzy control base rule. When the input and output variables and membership functions are specified, the rule-base (or decision matrix of the fuzzy knowledge-base), composed of expert rules (if . . . , then. . .), can be designed. Depending on the number of membership functions for the input and output variables, it is able to define more or less potential rules. The easier case is a rule-base concerning only 1 input and 1 output variable. The fuzzy control scheme is realized in the inference engine, which is a base rule including all of the possible combinations of the inputs and the appropriate outputs for each of them [26–28].

8.3. Fuzzy inference

The basic operation of the inference engine is that it infers a logical deduction from evidence or information. This expresses that the fuzzy inference engine handles inference rules where human experience can simply be added through linguistic rules [26–28].

8.4. Defuzzification

In this part, a "crisp" numeric value used as a control input for the power system is produced by the outputs of the fuzzy rules. Once the input variables are fuzzified and sent to the fuzzy base rule, the fuzzy conclusion of the inference engine is defuzzified. A common technique, namely the centroid method, is employed for this aim, where the control signal is computed as [26–28]:

$$\Delta u = \sum_{i=1}^{n} \frac{F_i S_i}{S_i} \tag{5}$$

Here F_i is the membership grade and S_i is the membership function singleton position.

In this paper, 2 types of FLDCs with a different number of membership functions have been applied to the control system of the TCSC. Finally, using the simulation results for the rotor speed deviation and torque between the generator and the LP turbine, the best kind of FLDC has been determined.

In the first type, the inputs and the single output are normalized for the base values defined for the system. The structure and number of the membership functions illustrate the fuzzy value of the controller (for the inputs and output). The Zmf and Smf (Z and S shape membership function) membership functions are utilized for the input and output fuzzy sets of the FLDC. The designed membership functions for $\Delta\omega$ and $\Delta\gamma$ as the inputs and Δu as the output are shown in Figures 8 and 9.

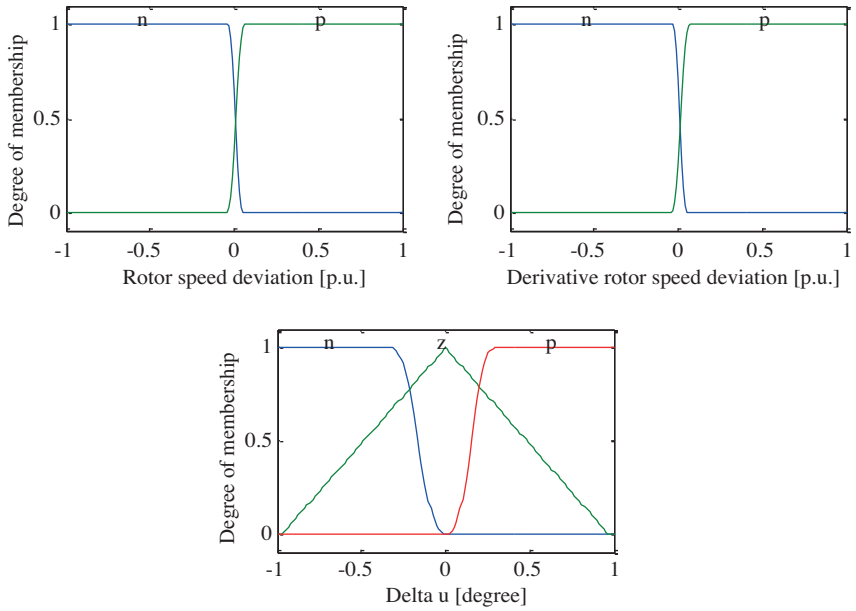

Figure 8. Membership functions for the input and output fuzzy adjustments of the first type of FLDC.

The control rules of the fuzzy controllers are presented by adjusting the innovative selected fuzzy rules. The fuzzy adjustments have been defined as: N: negative, Z: zero, and P: positive. The base rule with the 2 proposed inputs is presented as:

1. If ($\Delta\omega$ is P) and ($\Delta\gamma$ is P) then (Δu is P).
2. If ($\Delta\omega$ is P) and ($\Delta\gamma$ is N) then (Δu is Z).
3. If ($\Delta\omega$ is N) and ($\Delta\gamma$ is P) then (Δu is Z).

4. If ($\Delta\omega$ is N) and ($\Delta\gamma$ is N) then (Δu is N).

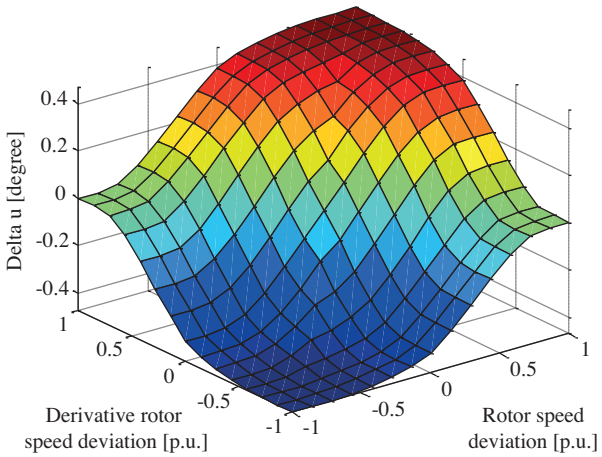

Figure 9. The designed fuzzy stabilizer rule surface of the first type of FLDC.

In the second type, the presented FLDC has a more complex structure. The membership functions of the input and output signals are shown in Figures 10 and 11. The Zmf and gaussmf (Z and gauss shape membership function) membership functions are utilized for the input and output fuzzy sets of this type of FLDC. There are 7 linguistic variables for each input variable and output variable, including, NL: negative large, NM: negative medium, NS: negative small, ZE: zero, PS: positive small, PM: positive medium, PL: positive large.

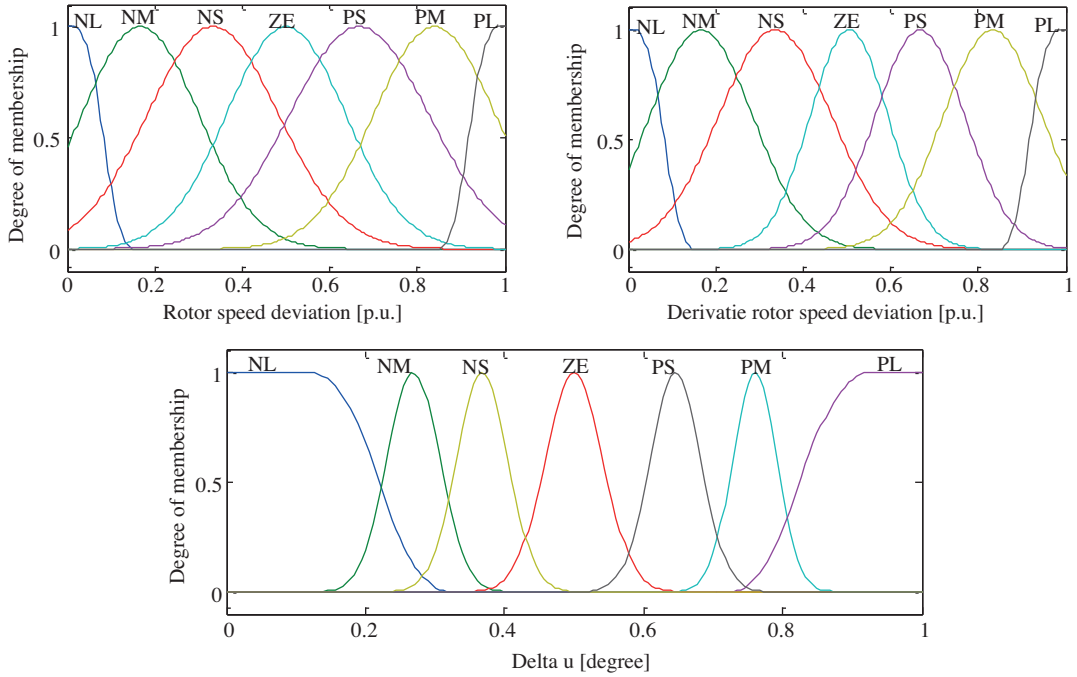

Figure 10. Membership functions for the input and output fuzzy adjustments of the second type of FLDC.

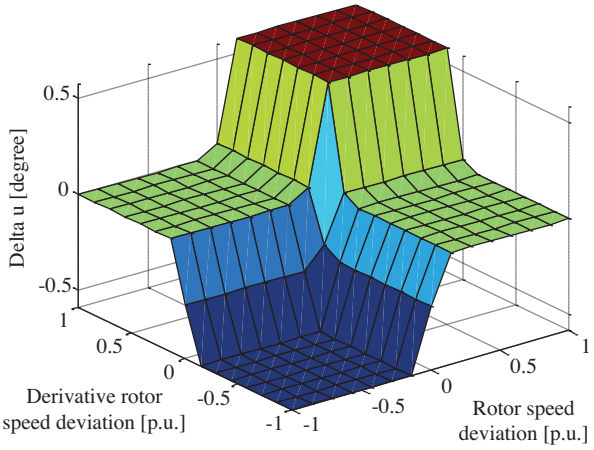

Figure 11. Designed fuzzy stabilizer rule surface of the second type of FLDC.

Table 3 shows the control roles of the fuzzy controllers that are demonstrated by a set of heuristically selected fuzzy rules.

Table 3. The rule bases used for the second type of FLDC.

Δω / Δγ	NL	NM	NS	ZE	PS	PM	PL
NL	NL	NL	NL	NL	NM	NS	ZE
NM	NL	NL	NL	NM	NS	ZE	PS
NS	NL	NL	NM	NS	ZE	PS	PM
ZE	NL	NM	NS	ZE	PS	PM	PL
PS	NM	NS	ZE	PS	PM	PL	PL
PM	NS	ZE	PS	PM	PL	PL	PL
PL	ZE	PS	PM	PL	PL	PL	PL

In previous sections, 2 types of FLDCs have been investigated. Now, in this section, with the presented simulation results for the rotor speed deviation and torque between the G and the LP turbine, which is shown in Figures 12a and 12b, it can be found that the first type has less overshoot and settling time compared with the second type. Moreover, the first type has a simple structure and fewer base rules than the second type.

9. Simulation results and discussion

The simulation results show the impact of the TCSC on the SSR damping and LFO by applying 2 kinds of faults using 2 control methods, the CDC and the FLDC.

Initially, the power system without any damping controllers is simulated when faults occur in bus 1 of Figure 1 at t = 0.7 s. The simulation results for the rotor speed deviation, torque between the G and the LP turbine, and the current line are shown in Figures 13a, 13b, and 13c. Due to the unstable mode, when the fault is cleared, large oscillations will be experienced between sections of the G turbine shaft. For this state, the system is completely unstable, and as depicted in Figure 2, the rotor speed is oscillating with a subsynchronous frequency of 25 Hz.

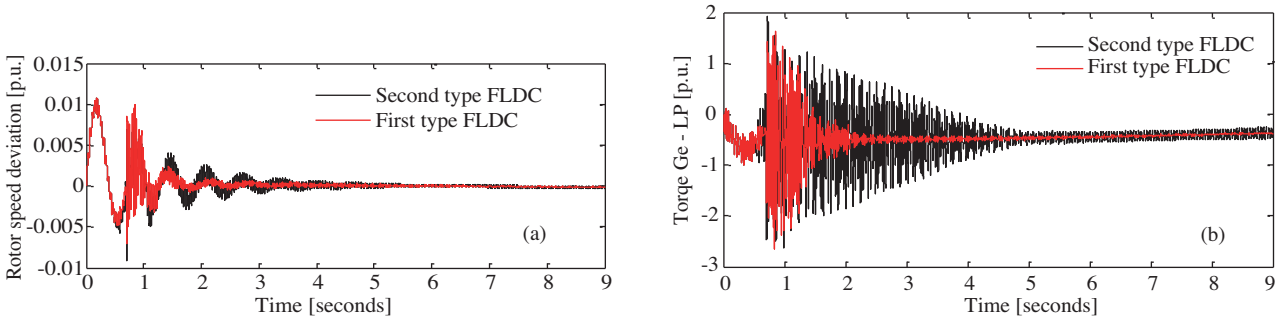

Figure 12. (a) Simulation results for the comparative between the first type of FLDC and the second type of FLDC: rotor speed deviation. (b) Simulation results for the comparative between the first type of FLDC and the second type of FLDC: torque between the G and the LP turbine.

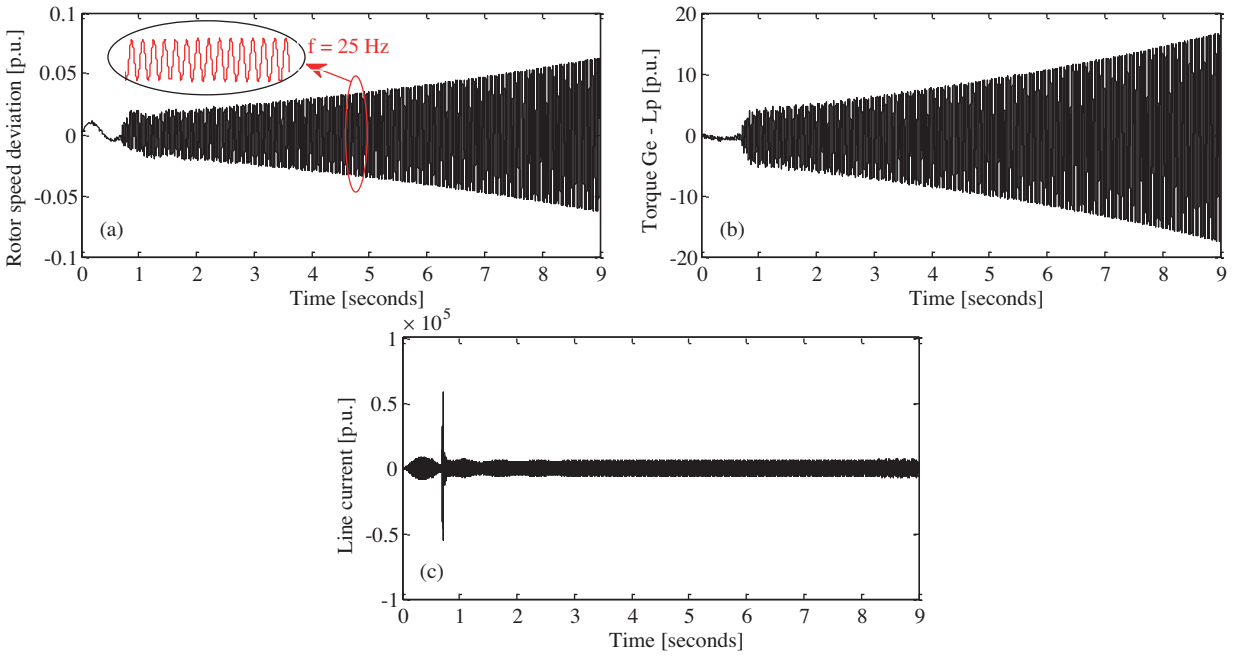

Figure 13. (a) Simulation results for the undamped condition: rotor speed deviation. Simulation results for the undamped condition: torque between the G and the LP turbine. (c) Simulation results for the undamped condition: line current.

As a result, for damping oscillations, the power system with a CDC and FLC in 2 cases is simulated. First, an inductive fault has been applied, followed by a resistive fault.

9.1. Case 1 : Simulation results with an inductive fault

In this case, an inductive fault happens by connecting a reactor at t = 0.7 s with a duration time of 16.9 ms. The simulation results are conducted with a TCSC in order to prove the effectiveness of the proposed FLDC and CDC optimized by the PSO algorithm in the SSR attenuation. Figure 14 shows that despite using the FLDC and CDC optimized by the PSO algorithm the inductive fault increased the line current from 25 kA to about 75 kA. The simulation results for the rotor speed deviation, the torque between the G and the LP turbine, and the line current are shown in Figures 14a, 14b, and 14c, where it is observed that the FLDC operates better

than the CDC optimized by the PSO algorithm, since the system with the FLDC has less overshoot and less settling time compared with the CDC.

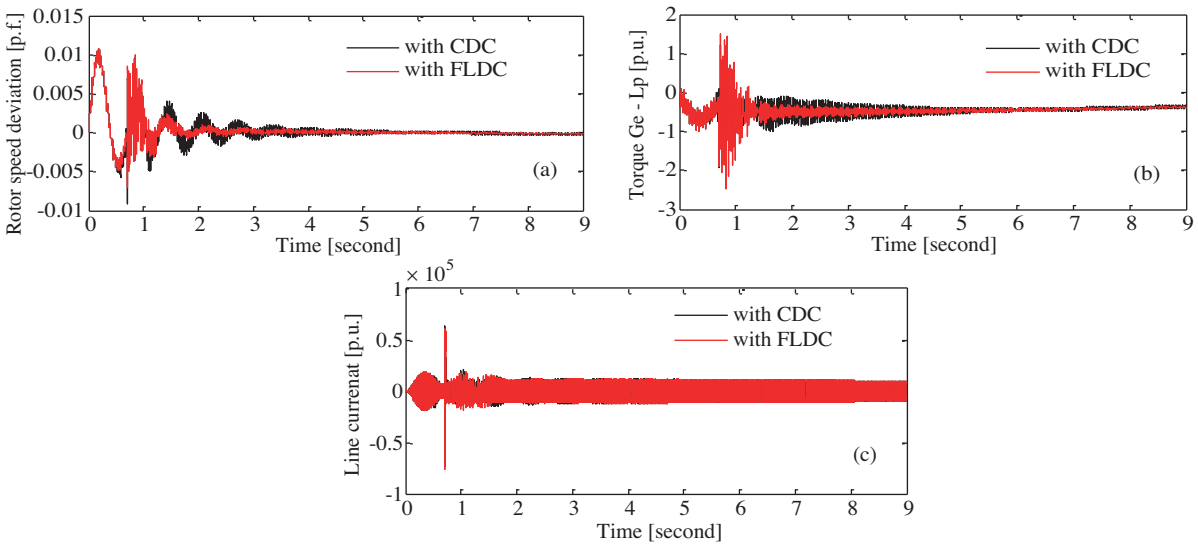

Figure 14. (a) Simulated results for the comparison between the CDC optimized by PSO and the FLDC with an inductive fault: rotor speed deviation. (b) Simulated results for the comparison between the CDC optimized by PSO and the FLDC with an inductive fault: torque between the G and the LP turbine. (c) Simulated results for comparison between the CDC optimized by PSO and FLDC with inductive fault: line current.

The FFT analysis on the generator rotor speed for the TCSC enhanced by FLDC is depicted in Figure 15. It is observed that the dominant torsional mode with a frequency of 25 Hz diminishes as time passes. Moreover, Figure 15 shows that between 0 and 3 s a low frequency power oscillation with a frequency of 1.5 Hz can be completely eliminated with the FLDC.

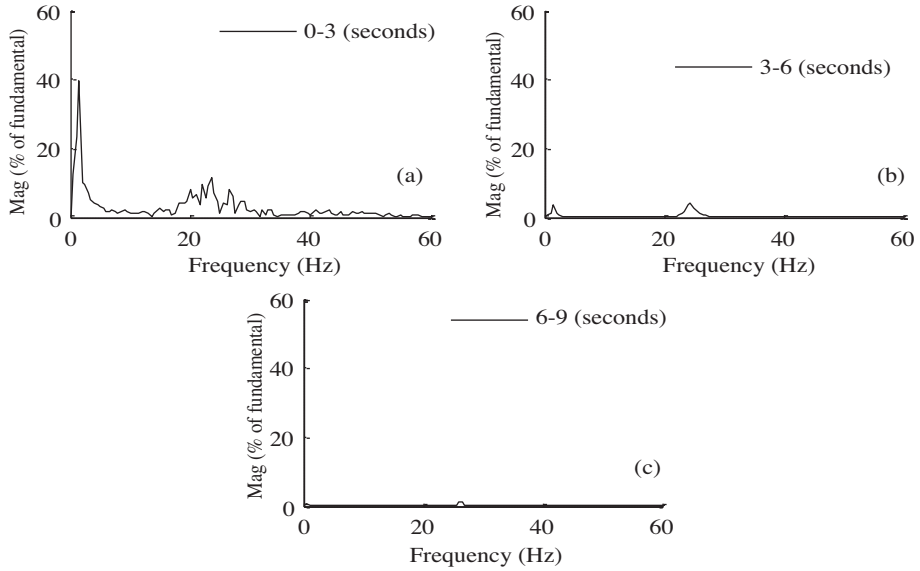

Figure 15. FFT analysis of the generator rotor speed with the FLC on the TCSC for the inductive fault.

9.2. Case 2: Simulation results with resistive fault

In this case, we applied a resistive fault at t = 0.7 s with a 20-ms duration. Again, like Case 1, the simulation results have been proposed with the CDC optimized by the PSO algorithm and FLDC. Figures 16a, 16b, and 16c show that despite using the CDC and FLDC the resistive fault increased the line current from 10kA to about 25kA. From Figures 16a, 16b, and 16c it is observed that the FLDC is found to be robust to the fault types and also has an excellent ability in damping the SSR and LFO in the power system compared with the CDC.

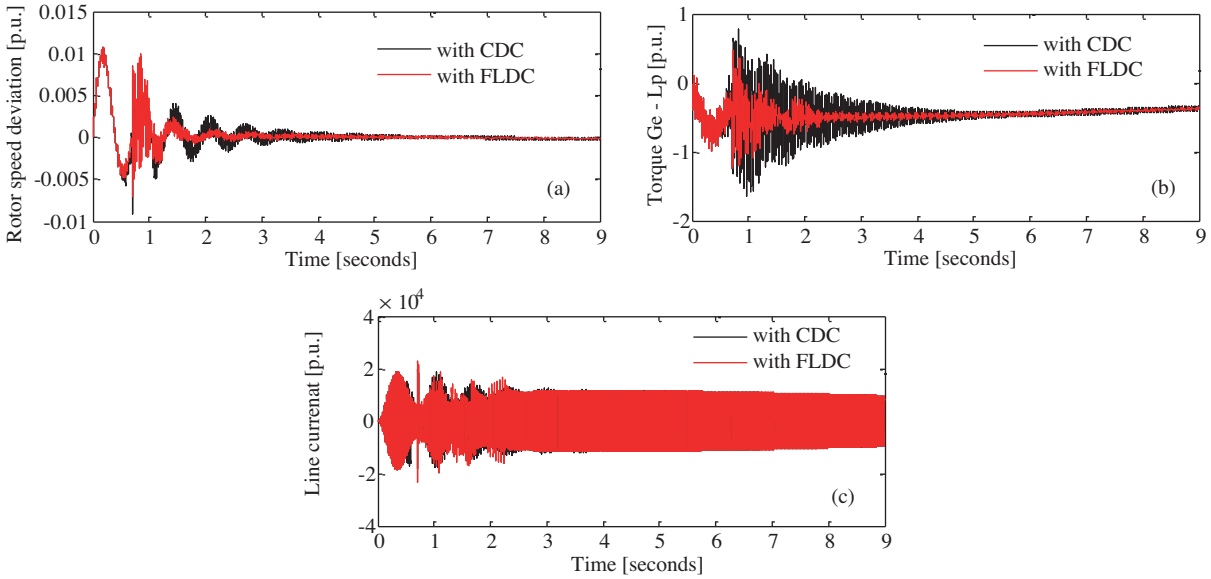

Figure 16. (a) Simulated results for the comparison between the CDC optimized with PSO and a FLC with a resistive fault: rotor speed deviation. (b) Simulated results for the comparison between the CDC optimized with PSO and a FLC with a resistive fault: torque between the G and the LP turbine. (c) Simulated results for the comparison between the CDC optimized with PSO and a FLC with a resistive fault: line current.

The results of the FFT analysis of Case2 are very similar to those of Case1, thus they have not been shown here.

10. Conclusions

In this paper, some performance results of the TCSC in the SSR and power oscillation damping in a highly unstable power system using simulation with MATLAB/Simulink have been shown. In order to make the TCSC able to mitigate the SSR in power oscillations, 2 control methods with the CDC and FLDC were investigated by applying 2 kinds of faults. First, simulations are carried out on an ISBM accumulated with a TCSC in 2 separate cases: Case 1 included the CDC and FLDC-based TCSC with the occurrence of an inductive fault and Case 2 included the CDC and FLDC-based TCSC with the occurrence of a resistive fault. In order to verify the better performance of the proposed FLDC toward conventional methods, the CDC is also designed and optimized with the PSO algorithm for damping the SSR and LFO. As it was illustrated, the FLDC's performance was more beneficial than that of the CDC, because the CDC's better operation is required to reach the suitable range of gains by repeating simulation more and more, while the proposed auxiliary fuzzy controller was adjusted in just a few simulations. The simulation results showed that the inductive fault is stronger than the resistive fault

and that the FLDC is robust to the fault types. Hence, it can be said the FLDC is a good candidate for the damping of the SSR and LFO in power systems compared with the CDC.

Nomenclature

f_e	Natural frequency
X_C	Reactance of the series capacitor
X_L	Reactance of the compensated line
f_o	Synchronous frequency
f_r	Complementary frequency
X_{fc}	Series-fixed capacitive compensation
$X_{TCSC}(\alpha)$	Equivalent reactance of the TCSC
ω	Generator rotor speed
$X_L(\alpha)$	Alterable inductive impedance of the TCR
α	Firing angle of the thyristor
α_{Clim}	Minimum firing angle of the thyristor in capacitive region
α_{Llim}	Maximum firing angle of the thyristor in the inductive region
$\Delta\omega$	Rotor speed deviation
$\Delta\gamma$	Derivative rotor speed deviation
Δ u	Output of the FLC
F_i	The membership grade
S_i	The membership function singleton position.

References

[1] P. Kundur, Power Systems Stability and Control, New York, McGraw-Hill, 1994.

[2] IEEE Committee Report, "Reader's guide to sub-synchronous resonance", IEEE Transactions on Power Systems, Vol. 7, pp. 150–157, 1992.

[3] IEEE Working Committee Report, "Third supplement to a bibliography for the study of sub-synchronous resonance between rotating machines and power systems", IEEE Transactions on Power Systems, Vol. 6, pp. 830–834, 1991.

[4] R.K. Varma, S. Auddy, "Mitigation of sub synchronous oscillations in a series compensated wind farm using static var compensator", IEEE Power Engineering Society General Meeting Conference, pp. 1–7, 2006.

[5] M. Bongiorno, J. Svensson, L. Angquist, "On control of static synchronous series compensator for SSR mitigation", IEEE Transactions on Power Electronics, Vol. 23, 2008.

[6] J. Guo, M.L. Crow, J. Sarangapani, "An improved UPFC control for oscillation damping", IEEE Transactions on Power Systems, Vol. 24, pp. 288–296, 2009.

[7] F.D. De Jesus, E.H. Watanabe, L.F.W. De Souza, J.E.R. Alves, "SSR and power oscillation damping using gate-controlled series capacitors (GCSC)", IEEE Transactions on Power Delivery, Vol. 22, pp. 1806–1812, 2007.

[8] D. Rai, G. Ramakrishna, S.O. Faried, A. Edris, "Enhancement of power system dynamics using a phase imbalanced series compensation scheme", IEEE Transactions on Power Systems, Vol. 25, pp. 966–974, 2010.

[9] A.D.D. Rosso, C.A. Canizares, V.M. Dona, "A study of TCSC controller design for power system stability improvement", IEEE Transactions on Power Systems, Vol. 18, pp. 1487–1496, 2003.

[10] K. Li, J. Zhao, C. Zhang, W. Lee, "Dynamic simulator for thyristor-controlled series capacitor", IEEE Transactions on Industry Applications, Vol. 46, pp. 1096–1102, 2010.

[11] D. Jovcic, G.N. Pillai, "Analytical modeling of TCSC dynamics", IEEE Transactions on Power Delivery, Vol. 20, pp. 1097–1104, 2005.

[12] K.M. Son, J.K. Park, "On the robust LQG control of TCSC for damping power system oscillations", IEEE Transactions on Power Systems, Vol. 15, pp. 1306–1312, 2000.

[13] L.A.S. Pilotto, A. Bianco, W.F. Long, A. Edris, "Impact of TCSC control methodologies on subsynchronous oscillations", IEEE Transactions on Power Delivery, Vol. 18, pp. 243–252, 2003.

[14] M. Noroozian, M. Ghandhari, G. Andersson, J. Gronquist, I. Hiskens, "A robust control strategy for shunt and series reactive compensators to damp electromechanical oscillations", IEEE Transactions on Power Delivery, Vol. 16, pp. 812–817, 2001.

[15] H.A. Mohammadpour, S.M.H. Mirhoseini, A. Shoulaie, "Comparative study of proportional and TS fuzzy controlled GCSC for SSR mitigation", IEEE Second International Conference on Power Engineering, Energy and Electrical Drives, pp. 564–569, 2009.

[16] A. Ajami, N. Taheri, M. Younesi, "A novel hybrid fuzzy/LQR damping oscillations controller using STATCOM", Second International Conference on Computer and Electrical Engineering, Vol. 1, pp. 348–352, 2009.

[17] K.R. Padiyar, Power System Dynamics: Stability and Control. Bangalore, Interline, 1996.

[18] E. Katz, "Sub-synchronous resonance", Paper presented at a panel discussion on Dynamic Stability in the Western Interconnected Power Systems, IEEE PES Summer Meeting, 1974.

[19] IEEE SSR Working Group, "Second benchmark model for computer simulation of Sub synchronous resonance", IEEE Transactions on Power Apparatus and Systems, Vol. 104, pp. 1057–1064, 1985.

[20] N.G. Hingorani, L. Gyugyi, Understanding FACTS: Concepts and Technology of Flexible AC Transmission System, New Jersey, Wiley-IEEE Press, 2000.

[21] R.M. Mathur, R.K. Varma, Thyristor-Based FACTS Controllers for Electrical Transmission Systems, New Jersey, Wiley-IEEE Press, 2002.

[22] H. SL, S. Yang, G. Ni, E.W.C. Lo, H.C. Wong. "A particle swarm optimization based method for multi objective design optimizations", IEEE Transactions on Magnets, 2005.

[23] R. Poli, J. Kennedy, T. Blackwell, "Particle swarm optimization: an overview", Swarm Intelligence, Vol. 1, 33–57, 2007.

[24] A. Ratnaweera, S.K. Halgamuge, H.S. Watson, "Self organizing hierarchical particle swarm optimizer with time varying acceleration coefficients", IEEE Transactions on Evolutionary Computation, Vol. 8, pp. 240–55, 2004.

[25] C.L. Phillips, J.M. Parr, "Robust design of a digital PID dedicator controller", IEEE Transactions on Industrial Electronics, Vol. 31, pp. 328–332, 1984.

[26] H. He, "Fuzzy modeling and fuzzy control [book review]", Computational Intelligence Magazine, IEEE, Vol. 3, pp. 8–10, 2008.

[27] H.J. Zimermann, Fuzzy Set Theory and its Applications, 3rd Edition, The Netherlands, Kluwer Academic Publishers, 1996.

[28] R. Langari, Fuzzy Control Synthesis and Analysis, New York, Wiley, 1995.